Performance of a Low-Cost Earthquake Early Warning System (*P*-Alert) and Shake Map Production during the 2018 M_w 6.4 Hualien, Taiwan, Earthquake

by Yih-Min Wu, Himanshu Mittal, Ting-Chung Huang, Benjamin M. Yang, Jyh-Cherng Jan, and Sean Kuanhsiang Chen

ABSTRACT

On 6 February 2018, an M_w 6.4 earthquake struck near the city of Hualien, in eastern Taiwan with a focal depth of 10.4 km. The earthquake caused strong shaking and severe damage to many buildings in Hualien. The maximum intensity during this earthquake reached VII ($> 0.4g$) in the epicentral region, which is extreme in Taiwan and capable of causing damage in built structures. About 17 people died and approximately 285 were injured. Taiwan was one of the first countries to implement an earthquake early warning (EEW) system that is capable of issuing a warning prior to strong shaking. In addition to the official EEW run by the Central Weather Bureau (CWB), a low-cost EEW system (*P*-alert) has been deployed by National Taiwan University (NTU). The *P*-alert network is currently operational and is capable of providing on-site EEW as well as a map of expected ground shaking. In the present work, we demonstrate the performance of the *P*-alert network during the 2018 Hualien earthquake. The shake maps generated by the *P*-alert network were available within 2 min and are in good agreement with the patterns of observed damage in the area. These shake maps provide insights into rupture directivity that are crucial for earthquake engineering. During this earthquake, individual *P*-alert stations acted as on-site EEW systems and provided 2–8 s lead time in the blind zone around the epicenter. The coseismic deformation (C_d) is estimated using the records of *P*-alert stations. The higher C_d values ($C_d > 2$) in the epicentral region are very helpful for authorities for the purpose of responding to damage mitigation.

INTRODUCTION

Located on the western circum-Pacific seismic belt, Taiwan is frequently struck by earthquakes. The collision between the nearby Philippine Sea plate (PSP) and Eurasian plates (EP) contributes to the complex geological features of Taiwan. To the east of Taiwan, the PSP subducts northward under the EP along the Ryukyu trench (Fig. 1a). To the southwest of Taiwan, the EP subducts eastward under the PSP (Tsai *et al.*, 1977; Wu *et al.*, 2008). Tectonically, most of Taiwan is under northwest–southeast compression, with a measured convergence rate of ~8 cm/yr (Yu *et al.*, 1997). The damaging earthquakes happening in Taiwan can be divided into two categories, those associated with the plate boundary and the others associated with active faults in western Taiwan (Wu *et al.*, 1999).

The Hualien earthquake is located in northeastern Taiwan, where seismic activity is due to the subduction of the PSP under the EP. In the neighborhood of the epicenter, there is the Milun fault (Fig. 1a). It caused an **M** 7.3 earthquake in October 1951, although it has not been active for the past two decades. A detailed study of in-land seismogenic features in Taiwan by Shyu *et al.* (2016) suggests that the region is a curved reverse-fault system. The system consists of two reverse faults, the Milun fault and the other east–west-striking reverse fault located offshore north of the Milun tableland (Fig. 1a).

The recent earthquake of 6 February 2018 may be associated with the Milun fault. The peak ground acceleration (PGA) at some stations recorded by the *P*-alert network reached around $0.6g$, giving rise to a maximum intensity of VII. This earthquake was well located by the Central Weather Bureau (CWB) (official agency in Taiwan). Based on the CWB rapid-reporting system (Wu *et al.*, 1997, 2000), the earthquake was located 18.3 km north-northeast of city of Hualien, with a focal depth 10.0 km. The Broadband Array in Taiwan for Seismology (BATS) and the U.S. Geological Survey (USGS) reported focal mechanisms for this event (Fig. 1a), and both confirm oblique slip faulting with two nodal planes striking northeast–southwest and northwest–southeast. The notion that the Milun fault is responsible for this earthquake is based on the structure and location of the Milun fault, which is mapped as a reverse fault with a strike-slip component. The obtained focal mechanism seems to support this finding. This earthquake caused severe damage to many buildings in the city of Hualien. About 17 people were reported dead and 285 injured (Wikipedia, 2018). Maximum causalities

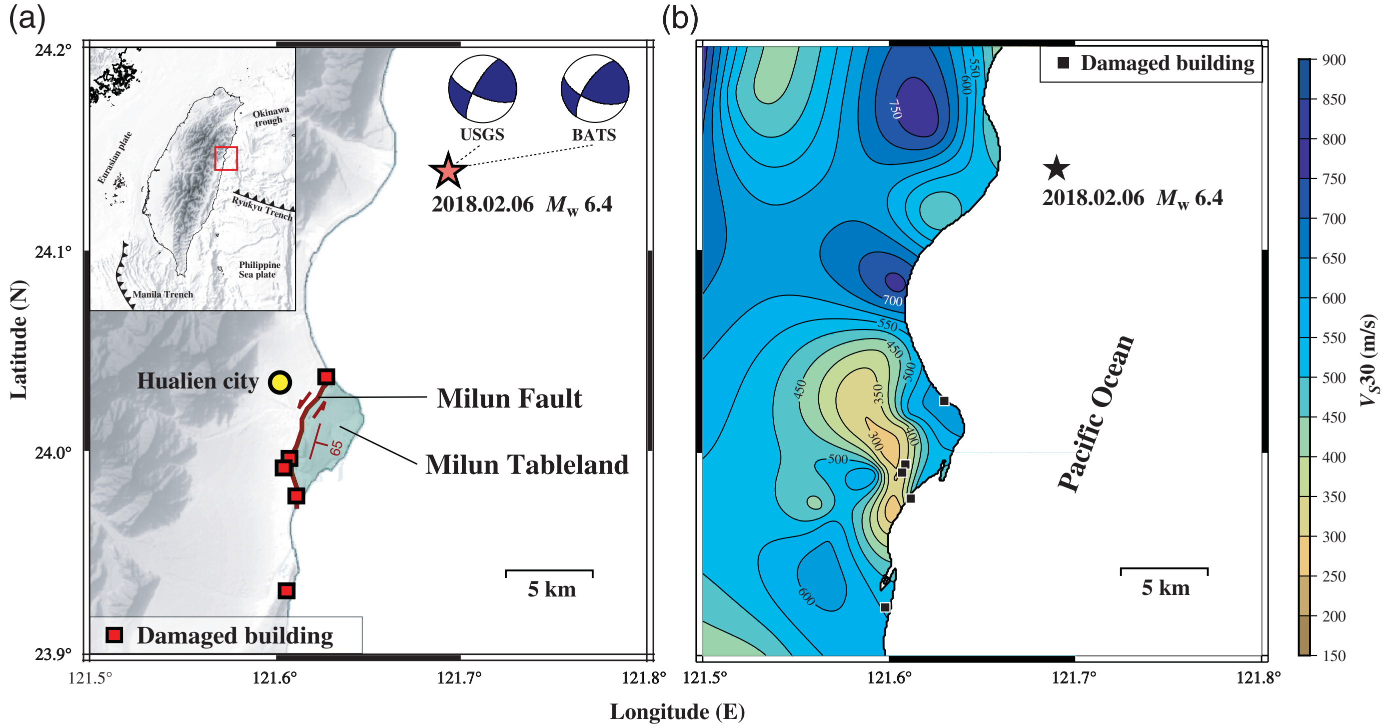

▲ **Figure 1.** (a) Tectonics map of the Taiwan region and Hualien area. The red line indicates the Milun fault. (b) V_{S30} map of the Hualien area. Stars show the epicenter of the 6 February 2018 M_w 6.4 Hualien earthquake, and squares show the buildings damaged by the Hualien earthquake.

were reported in a 12-story residential building that tilted due to collapse of some lower floors. Correlation of this earthquake with the Milun fault is also supported by the damage pattern of buildings that are within a few hundred meters of this fault. Although five of the collapsed structures are in the vicinity of the Milun fault, soil liquefaction and resonance may also play a role because the city of Hualien is built on deep sediment (Fig. 1b). This earthquake occurred 2 yrs after the 6 February 2016 Meinong earthquake that killed 117 people (Wu *et al.*, 2016) in southern Taiwan. Wu *et al.* (2016) reported the performance of the *P*-alert network-based earthquake early warning (EEW) system during this earthquake.

Taiwan was one of the first countries to implement an EEW system that is capable of issuing a warning prior to strong shaking. The CWB only issues regional warnings for cities more than 50 km away from the epicentral region. For cities within 50 km, an on-site EEW system would be helpful. In addition to the official EEW of CWB, a low-cost *P*-alert system deployed by National Taiwan University (NTU) is in operation and is capable of providing on-site EEW, as well as rapid shake maps. This network consists of 636 *P*-alert stations. This network was initiated by a research group at NTU and is based on low-cost microelectromechanical system (MEMS) accelerometers (Wu *et al.*, 2013; Wu, 2015). The NTU group is also helping other countries build their own EEW networks using *P*-alert. Most recently, a network of 100 *P*-alert instruments was installed in one portion of the Himalayan belt of India (Kumar *et al.*, 2014), where large earthquakes pose great danger to people living in the plains (Mittal *et al.*, 2013, 2016). During the Hualien earthquake, the *P*-alert system performed very well and recorded good-quality data. A detailed shake map was provided by the *P*-alert network within 2 min of the occurrence of the Hualien earthquake. The areas with maximum values of PGA and peak ground velocity (PGV) show some correlation with the damaged areas. For example, the damaged buildings are located in the area where PGV is maximum. The network also has the capability to image rupture directivity, a key parameter in damage assessment; stations in the direction of propagation of the rupture front will record larger acceleration or velocity values, whereas stations in the other directions will observe smaller values. This phenomenon was well documented in previous studies (Hsieh *et al.*, 2014; Wu, 2015). For regional EEW, signals are transferred continuously from field stations to a central recording station situated at NTU, as well as at Institute of Earth Science, Academia Sinica (IESAS) for research purposes. In addition to regional EEW, individual *P*-alert stations act as on-site EEW systems and provide warnings when predefined thresholds are exceeded (Wu *et al.*, 2011, 2013; Hsieh *et al.*, 2015). In this article, we examine the data obtained from the *P*-alert network and its performance during the Hualien earthquake.

P-ALERT NETWORK

The *P*-alert seismic network is a dense array of 636 stations in Taiwan (Fig. 2). As mentioned earlier, these sensors are low-cost MEMS-based acceleration sensors introduced in

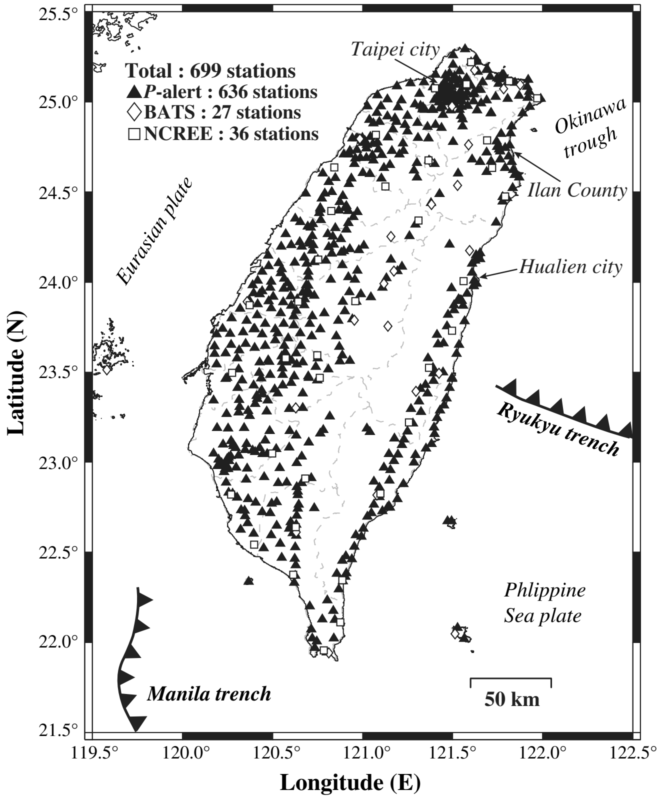

▲ **Figure 2.** Station distribution of the *P*-alert network along with the Broadband Array in Taiwan for Seismology (BATS) and National Center for Research on Earthquake Engineering (NCREE) real-time strong-motion networks.

the early 1990s (Holland, 2003). Encouraged by its cost and efficiency, people at NTU started a pilot project in which 15 *P*-alert instruments were installed in the eastern part of Taiwan (Wu and Lin, 2014). Coincidentally, Hualien was the area where *P*-alerts stations were installed for the first time. Based on the performance of these instruments, this network was later extended to other parts of Taiwan as well (Wu *et al.*, 2013, 2016; Wu, 2015). At present, *P*-alert stations are installed densely (almost every 5 km) in every populated part of Taiwan. Most of the *P*-alert stations are installed in two- or three-story buildings (preferably schools), where suitable power and internet connectivity is available. Because *P*-alert instruments are installed in the buildings, the site effects and soil–structure interaction also affect the PGA recorded by these instruments. Real-time signals from these instruments are continuously transferred to a server station at NTU and IESAS, where these data are stored and processed using Earthworm software (Johnson *et al.*, 1995; Chen *et al.*, 2015). Data from the *P*-alert network is augmented by real-time strong-motion data from a network of 36 stations of the National Center for Research on Earthquake Engineering (NCREE) and another network of 27 stations from BATS, collectively forming a network of 699 stations. The station distribution for all three kinds of instrumentation is shown in Figure 2.

Each *P*-alert instrument provides three-component data with a sampling frequency of 100 Hz. The system is designed to have 16-bit resolution and a $\pm 2g$ clip level. *P*-alert has a low-pass filter that can be configured for 10 or 20 Hz. The data received by each *P*-alert instrument in the field is processed to obtain the vertical peak displacement P_d for on-site EEW (Wu and Kanamori, 2005). The process of estimating P_d follows a two-stage integration process with a 0.075 Hz high-pass filter (Shieh *et al.*, 2008). Once the predefined thresholds, that is, $P_d > 0.35$ cm or PGA $> 0.08g$ (the CWB intensity V threshold), are exceeded, an on-site warning is generated (Wu *et al.*, 2011). The CWB intensity V is defined by PGA between 0.08 and $0.25g$, and can cause light damage. According to Wu and Kanamori (2005), a P_d of 0.35 cm corresponds to a PGV of 17 cm/s, and according to Wu *et al.* (2003) CWB intensity V corresponds approximately to a PGV between 17 and 49 cm/s. The data are transferred to the NTU office and are processed for regional warning as well as the generation of real-time shake maps. The regional warning generated by this network is currently used for research work; the CWB is the official agency in Taiwan issuing regional warnings. For the Hualien event, both the *P*-alert and CWB networks provided regional warnings within 15 s after an earthquake occurrence.

SHAKE MAP

Once 12 instruments are triggered with a PGA of $0.0012g$, the *P*-alert network starts plotting shake maps. These shake maps are updated every minute as long as other instruments are triggering, and the maps are delivered automatically via e-mail to concerned persons, including the National Science and Technology Center for Disaster Reduction (NCDR), to provide adequate time for relief work. These shake maps are automatically posted on the official *P*-alert webpage on Facebook. The Hualien earthquake happened at 23:50:42.6 (local time), and the first PGA shake map was posted on Facebook at 23:50:48, roughly 6 s later, based on data from 76 instruments (Fig. 3a). This shake map was updated every minute following the earthquake. The shake map was last updated 7 min later, at 23:57:08, based on data from 539 instruments. Figure 3 shows the near-real-time shake maps generated by the *P*-alert network during this event. At the time the first shake map was generated, only the instruments closest to the epicenter had attained maximum PGA values. Because the outermost instruments have not yet recorded their maximum accelerations, the outermost contours are absurd. Figure 3b shows the final shake map delivered for the Hualien earthquake using all triggered *P*-alert instruments. In total, 539 instruments triggered and contributed to the shake map.

Figure 4 compares PGA and PGV shake maps using combined data from *P*-alert, BATS, and NCREE with the CWB PGA shake map. We employ the distance inverse method to interpolate the shake map, which is in accordance with the previous study (Yang *et al.*, 2018). The different interpolation schemes used by different versions of ShakeMap are well documented. Worden *et al.* (2010) describe the interpolation

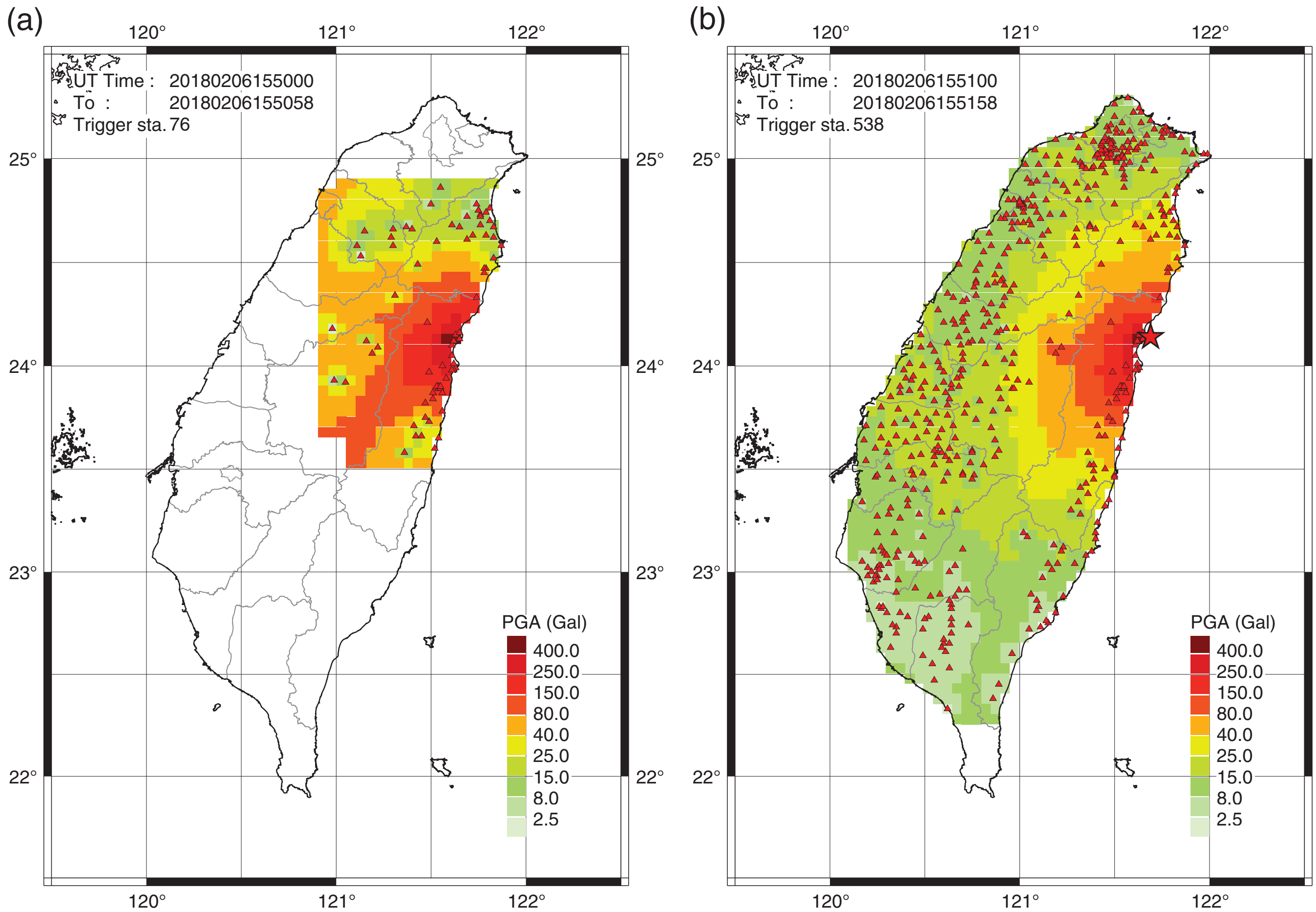

▲ **Figure 3.** Peak ground acceleration (PGA) shake map of the 6 February 2018 M_w 6.4 Hualien earthquake produced by the *P*-alert network. (a) The first shake map after 6 s of the earthquake occurrence with the triggering of 76 instruments. (b) The shake map after all available *P*-alert instruments have triggered.

procedure used in ShakeMap 3.5, but it was found to have serious issues so the methodology was overhauled in ShakeMap 4 (Worden *et al.*, 2018). One of the improvements in Worden *et al.* (2018) was to eliminate the parameterization of their smoothing/interpolation using a radius of influence (ROI = 10 km); this eliminated islands near stations with peak ground-motion outliers.

The results in our case demonstrate that, although the shape of shaking contours is the same for the two networks, the combined networks' PGA shake map is smoother than the CWB network. The CWB network provides a shake map based on 110 real-time instruments, so the distribution of contours is more scattered and unreasonable. *P*-alert instruments are less densely installed in the area near Hualien, as compared to other parts of Taiwan, because of difficult logistics in mountain areas. However, the shake map generated by the combined networks is more reasonable because much less interpolation is needed. For example, there are four or five spurious 0.4*g* contours or islands in the CWB shake map. These contours could not be smoothed because the interpolation is based on the instruments placed within a 5 km range. On the other hand, the addition of a few *P*-alert instruments close to the epicenter means that smooth contours are obtained. In the same way, the 0.25*g* contour for CWB shake map is based on data received from two or three instruments, whereas the combined-data shake map generates the same contour using data from nearly 15 instruments. Toward city of Taipei in the north, the observed PGA values using combined data are found between 0.008*g* and 0.025*g*, whereas for CWB network at the same places, observed PGA values are found to be less than 0.008*g*. All these differences in PGA contours may be attributed to sparse instrumentation of the CWB.

ON-SITE EEW

The CWB takes around 15 s to issue a regional warning (Chen *et al.*, 2015) and does so only for cities at least 50 km away from the epicentral region. Lead time in Taiwan may range from a few seconds to 30 s, depending on the distance from the epicenter. The lead time at a particular location is defined as the time gap between the issuing of warning and the arrival of strong shaking (maximum PGA or PGV). For cities located within 50 km, no regional warning is possible; this is the blind zone. Because the *P*-alert system is capable of issuing both

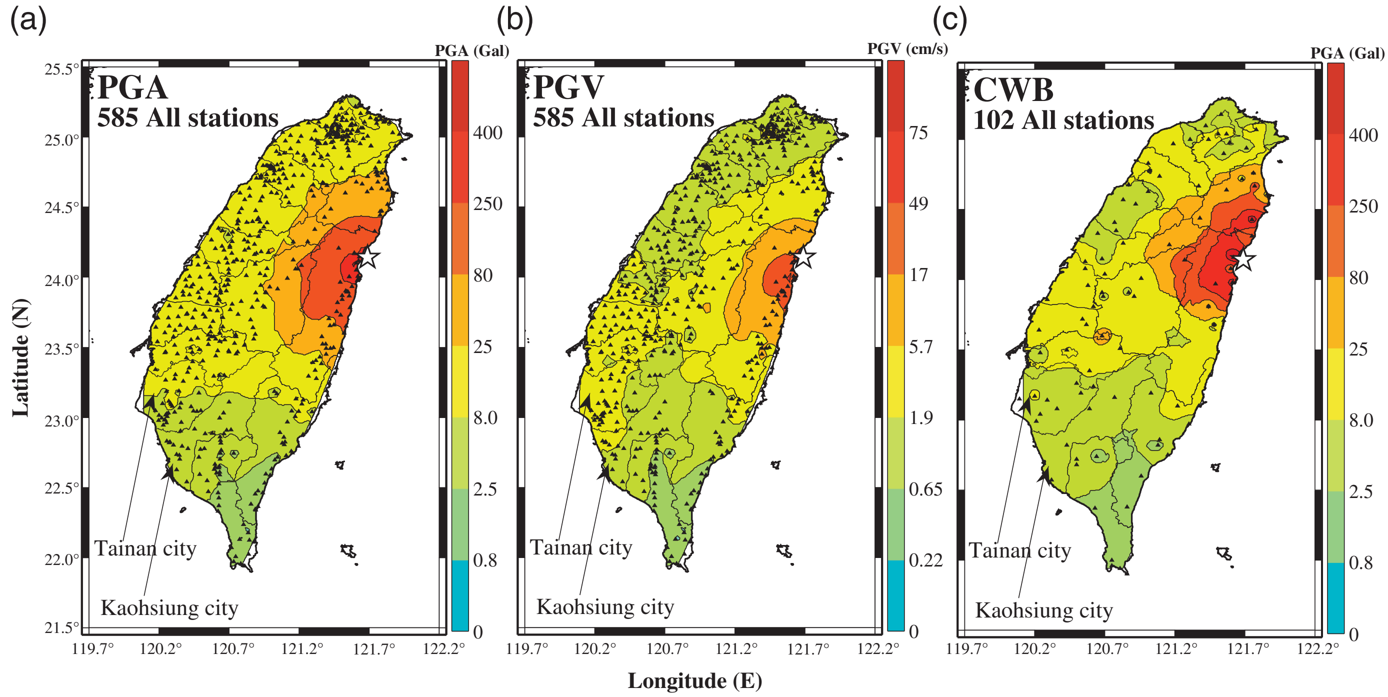

▲ **Figure 4.** Comparison of shake maps from the combined (*P*-alert, BATS, and NCREE) networks and Central Weather Bureau (CWB) stations alone. (a) PGA shake map from combined networks. (b) Peak ground velocity (PGV) shake map from combined networks. (c) PGA shake map from CWB stations alone.

on-site and regional warnings, *P*-alerts installed in the blind zone alleviate this problem. Each *P*-alert in the blind zone acts as an individual EEW system and issues a warning when the PGA or P_d is greater than 0.08*g* or 0.35 cm, respectively (Wu and Kanamori, 2005; Wu *et al.*, 2011). The *P*-alert network worked very well for on-site warning during the Hualien earthquake and provided useful lead time.

Figure 5 shows the lead time for PGA and PGV around the epicenter. The warning time for PGA or PGV ranges from 1.5 to 8 s. The closest instruments to the epicenter are W011 and W029, where PGA lead time is 1.1 and 2.1 s, respectively. In the same way, PGV lead time for these two stations is found to be 1.7 and 3.0 s, respectively. The average PGA lead time for instruments in the blind zone is 4.5 s, whereas for PGV it is 4.2 s. The instruments placed closest to the damaged building that caused 17 fatalities reported relatively high lead times (6–8 s).

DATA QUALITY OF *P*-ALERT NETWORK

The *P*-alert instruments recorded timely, good-quality data during this earthquake. Almost all the instruments placed in the vicinity of the epicenter transferred data to the central station without gaps. This represents a significant improvement since the the Meinong earthquake of 2016, when some of the stations provided only the initial few seconds of data and lost the rest of the data because of a break in internet connectivity (Wu *et al.*, 2016). Figure 6 shows three-component time series from *P*-alert stations close to the epicenter. Though high PGAs were recorded at instruments close to the epicenter, the corresponding PGVs at these stations are reduced, as compared to other stations southwest of the epicenter where buildings were damaged. This finding reinforces the notion that PGV is a better indicator of building damage than PGA (Wu *et al.*, 2004, 2016). Fling effect characterized by a large amplitude velocity pulse and a monotonic step in the displacement time history (Kalkan and Kunnath, 2006) is clearly visible in velocity traces close to the damaged area.

The *P*-alert data can be used efficiently in many applications other than EEW and shake-map generation. Yin *et al.* (2016) and Hsu *et al.* (2018) used *P*-alert data for structural health monitoring (SHM), whereas Jan *et al.* (2017) used these data to estimate coseismic deformation (C_d) using a two-stage baseline and integration approach (Wu and Wu, 2007). Jan *et al.* (2017) computed C_d values using records from *P*-alert stations and compared them with C_d values from Global Positioning System data and records from the Taiwan Strong Motion Instrumentation Program. The results match well. Figure 7 shows the C_d value obtained from two stations, W002 and W028, close to the damaged-building area. C_d reached 57.80 ± 4.50 cm on the east–west (EW) component and 14.05 ± 2.53 cm on the Z component at W002. In same way, at W028, 61.45 ± 5.01 cm was observed on the north–south (NS) component and 6.50 ± 0.94 cm on the Z component. High C_d estimates ($C_d > 2$ cm) in the epicentral region based on *P*-alert data can help authorities respond appropriately for the purpose of emergency response and damage mitigation. Figure 8 shows a section plot of traces from the *P*-alert

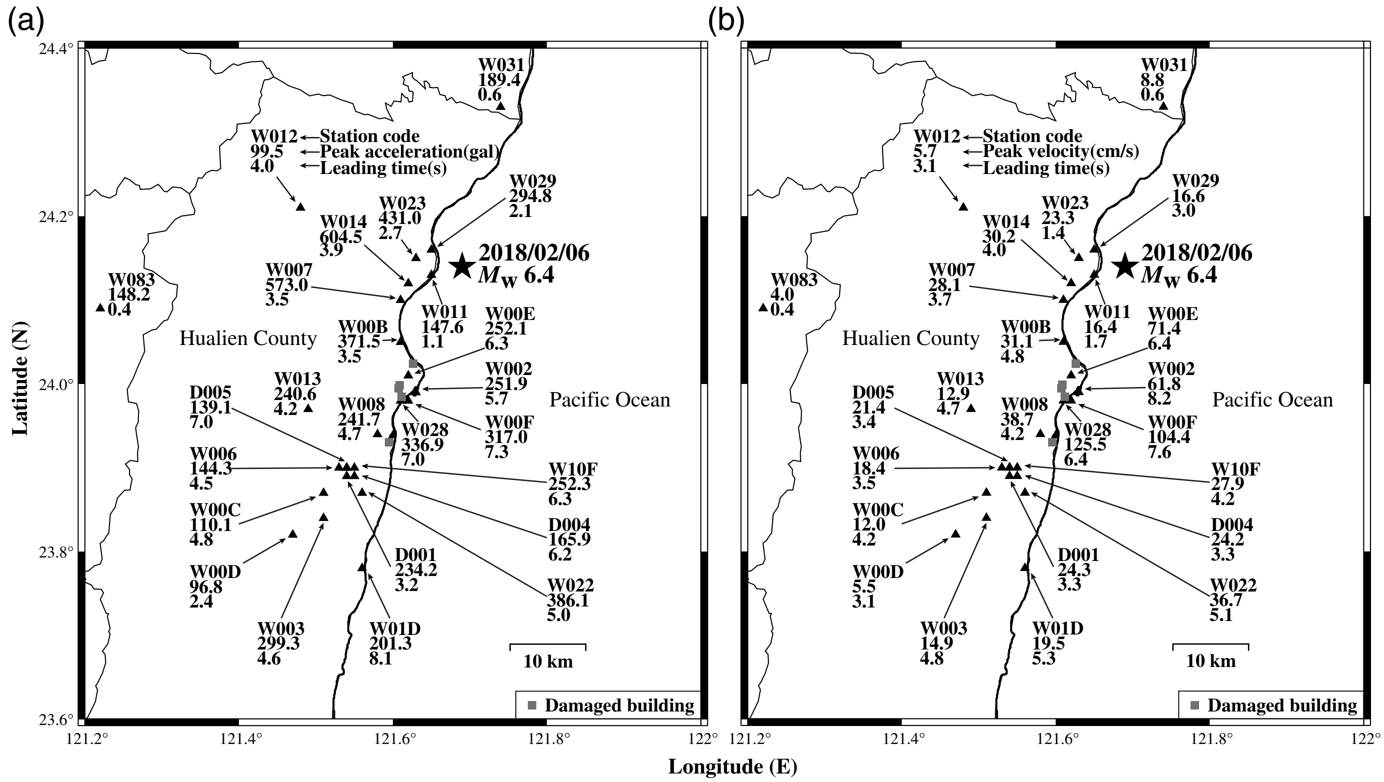

▲ **Figure 5.** Early warning lead time distribution for the *P*-alert network during the Hualien earthquake. (a) Lead time based on PGA. (b) Lead time based on PGV. Solid squares show the location of the damaged buildings.

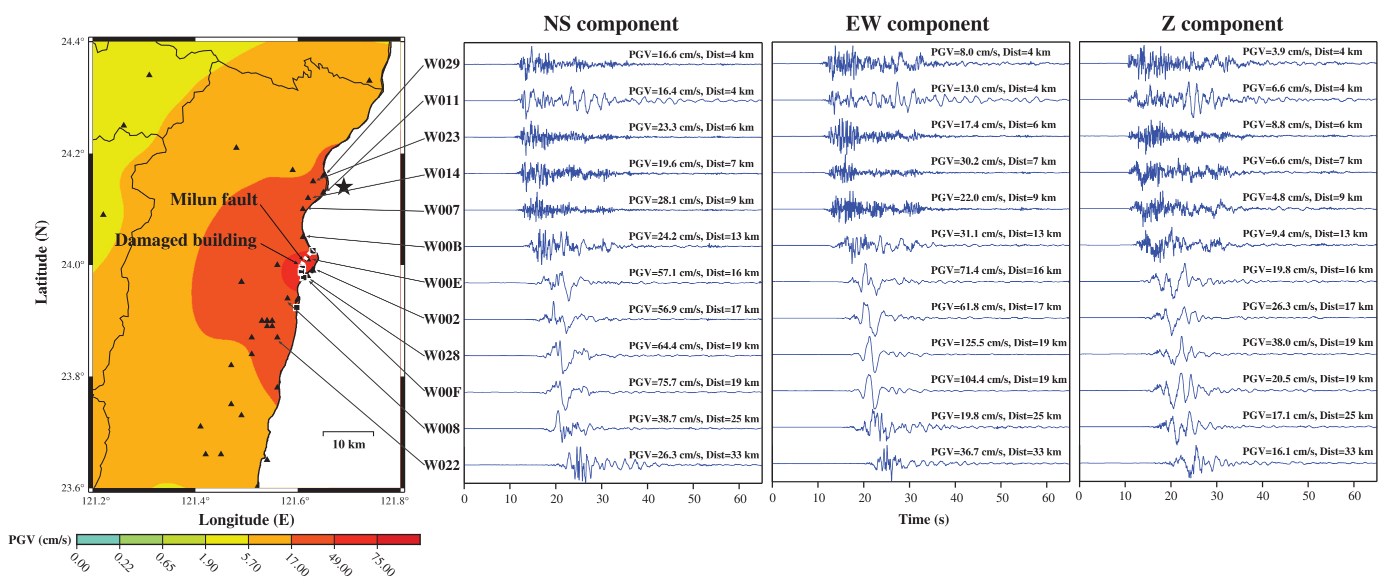

▲ **Figure 6.** A series of velocity traces recorded by *P*-alert during the Hualien earthquake. They represent the data quality of the network for north–south (NS), east–west (EW) and Z components.

network. After applying a Gaussian filter with a 0.2 Hz cutoff, a series of surface wave appears, with dispersion in time for traces away from the epicenter. This suggests that the records obtained from *P*-alert network can be used in surface-wave inversion as well.

DISCUSSION AND CONCLUSIONS

The first *P*-alert stations were installed in 2010 in the Hualien area (Wu and Lin, 2014). Encouraged by the network's efficiency and robustness, it was extended to other areas of

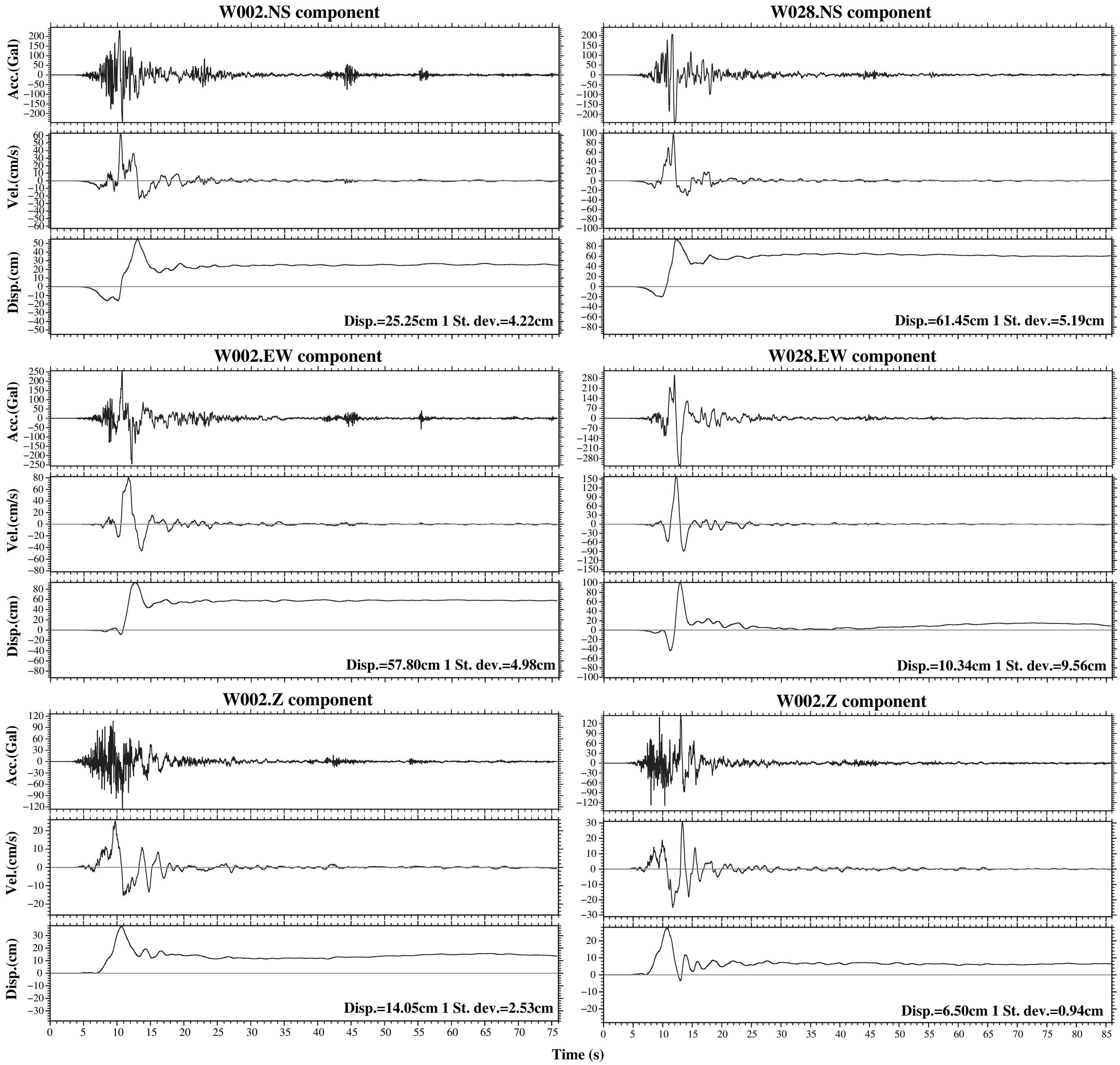

▲ **Figure 7.** Coseismic deformation at stations W002 and W028 during the Hualien earthquake.

Taiwan. Since then, the network has recorded some moderate-to-large earthquakes and many small earthquakes. Its performance during previous moderate earthquakes has been described earlier in other studies (Wu *et al.*, 2013, 2016; Hsieh *et al.*, 2014; Wu, 2015). The number of instruments is increasing every year. Two years ago, at the time of the 2016 Meinong earthquake, 581 *P*-alerts were installed in Taiwan; to date, that number has increased to 636. It is the low cost (around one-tenth of a traditional accelerometer) that allows us to expand this network.

The 2018 Hualien earthquake was the first destructive earthquake after the Meinong earthquake of 2016 to be widely recorded by the *P*-alert network. PGA shake maps were delivered in real time following this earthquake (Fig. 3). Later, these data were augmented by the data from NCREE and BATS instruments to produce PGA (Fig. 4a) and PGV (Fig. 4b) shake maps. Figure 4c shows the PGA shake map produced by the 110 instruments of CWB network. Although both networks show similar patterns in the contour map of PGA, that produced by combined networks looks more reasonable, considering the smoothness of PGA contours. The area between $0.025g$ and $0.25g$ contours in CWB shake map shrinks toward south because of the low density of instruments in that area. These maps provide insight about PGA and shaking intensity,

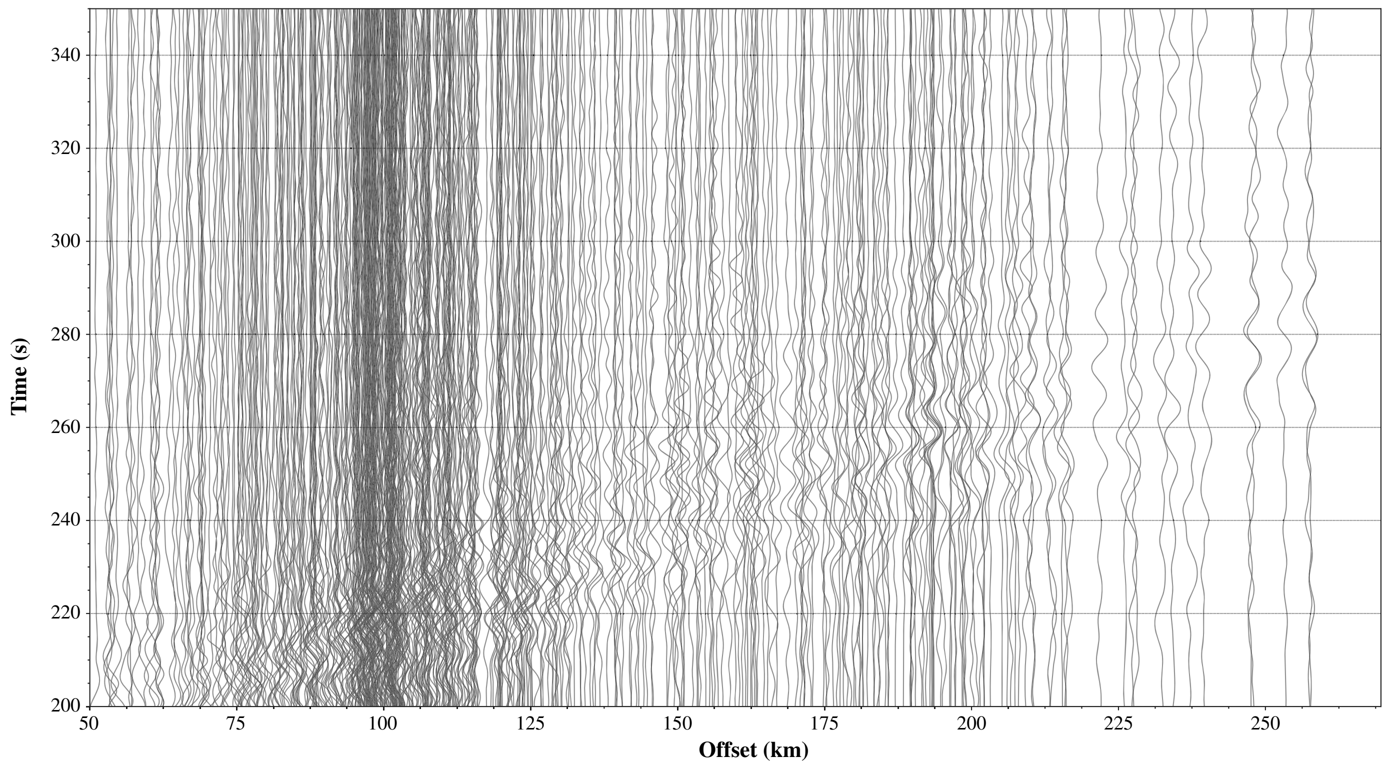

▲ **Figure 8.** Section plot of *P*-alert traces. The signature of the surface wave is evident, including dispersion.

allowing authorities, including NCDR, to conduct rapid loss assessments following a destructive earthquake.

The maximum intensities were reported in central Hualien County and the nearby Yilan County, where the shaking intensity reached VII (> 0.4*g*), as reported by the CWB. Five buildings (shown as squares in Fig. 9) were structurally damaged in the Hualien area. This earthquake caused 17 fatalities and several injured. A 12-story building tilted to a dangerous angle because of this event, claiming many lives. The damaged buildings are located in an area of high PGV (> 49 cm/s, see Fig. 9). This seems quite different from the 2016 Meinong earthquake (Wu *et al.*, 2016), where buildings collapsed in the areas of PGV around 17 cm/s. One possible explanation for this is that the structural quality in the Hualien area is much better than in the Tainan area. Only one or two buildings falling in the zone of PGV > 17 cm/s suffered structural damage during the Hualien earthquake. Though the magnitudes of both the 2016 Meinong earthquake and the 2018 Hualien earthquake were similar, less destruction was reported during the Hualien earthquake. This difference may be attributed to the deeper sediment accumulation in the Tainan area as compared to Hualien. A strong energy pulse is observed at 2.5 s, at which PGA almost reached around 0.4*g* and PGV has a pulse-like phase of about 100 cm/s or more at the period of 1–2 s (Fig. 6). Assuming a rupture velocity of 3.5 km/s and a strong energy pulse at 2.5 s, the asperity would be about 8 km (Ruiz *et al.*, 2011) from the epicenter and could be just underneath the damaged buildings.

Shake maps are also helpful in identifying rupture direction (Wu, 2015; Wu *et al.*, 2016; Legendre *et al.*, 2017). The focal mechanism for this event was released by BATS and USGS a few minutes after the occurrence of the earthquake. According to the focal mechanism provided by BATS and USGS, the two nodal planes are striking in the northeast–southwest and the northwest–southeast directions. The maximum PGV is found at stations southwest of the epicenter. Also, the aftershock distribution is concentrated toward the southwest (Fig. 9a). Comparing PGA and PGV shake maps with the focal mechanism and the aftershock sequence, it is clear that the more likely fault plane is northeast–southwest, where the aftershock sequence fits the shape of the shaking contours. This finding confirms the destruction in the city of Hualien, which is situated in southwest of epicenter. It is also confirmed by rupture slip inversion from waveform modeling (Lee *et al.*, 2018).

The data for research work from the *P*-alert network can be downloaded from an open website (shown in Data and Resources). The data are in Seismic Analysis Code format in units of cm/s^2 and polarity positive in vertical, north, and west. Most of the *P*-alert stations are installed in schools, so warnings were confined to schools. Because this earthquake occurred during the night, the maximum potential benefit of the network was not achieved. If the earthquake had happened during daytime, alarms would have gone off in the schools, and children are well trained to respond to such panic situations in Taiwan because earthquake drills are conducted frequently. If *P*-alert stations were installed more densely, for example, if it they were required

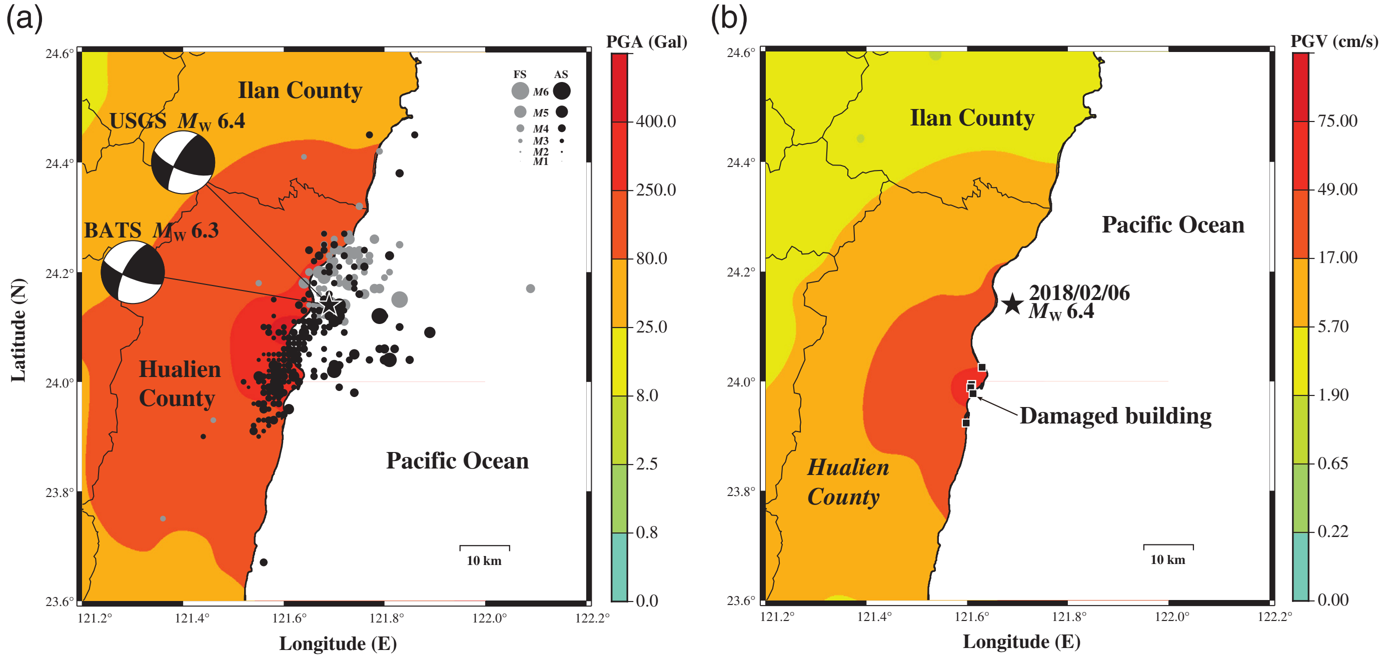

▲ **Figure 9.** (a) PGA shake map with focal mechanisms, foreshock, and aftershock sequence. (b) PGV shake map.

in all high-occupancy commercial buildings, on-site EEW in the blind zones could save many lives.

In conclusion, we report the performance of the *P*-alert network during the 2018 Hualien earthquake, an event that caused severe shaking in northeastern Taiwan. Overall, the results are quite satisfactory. The automatically generated shake map faithfully depicted the shaking resulting from the earthquake. The first PGA shake map was posted on Facebook, roughly 6 s later after the earthquake, with the triggering of 76 instruments. The final shake map got updated 7 min later, with the triggering of 539 instruments. These timely shake maps provided adequate time to NCDR for relief work. The on-site EEW has around a 2–8 s lead time, considering the relative lower density deployed in eastern side. In terms of data availability, no outages were suffered during this event. In fact, the data quality is so high that it can be used for other seismological studies, including SHM and estimation of C_d. The *P*-alert seismic network is robust and functions as needed during severe shaking.

DATA AND RESOURCES

The strong-motion waveform records used in this study were obtained from the National Taiwan University (NTU), the Institute of Earth Sciences (IES) of Academia Sinica, and the National Center for Research on Earthquake Engineering (NCREE) of Taiwan. The Generic Mapping Tools (GMT) software from Wessel and Smith (1998) was used in plotting part of the figures and is gratefully acknowledged. The official page of *P*-alert shake map on Facebook is at https://www.facebook.com/Palert. Shakemap/ (last accessed August 2018). The strong-motion waveform records for research work from *P*-alert network can be downloaded at http://palert.earth.sinica.edu.tw/db/ (last accessed August 2018).

ACKNOWLEDGMENTS

authors are profusely thankful to the Ministry of Science and Technology (MOST) in Taiwan for funding the project (MOST 106-2116-M-002-019-MY3), under which this study was carried out. This work was also financially supported by the National Taiwan University (NTU) Research Center for Future Earth from The Featured Areas Research Center Program within the framework of the Higher Education Sprout Project by the Ministry of Education (MOE) in Taiwan. The constructive comments from Editor-in-Chief Zhigang Peng and one anonymous reviewer helped in improving the article. Authors are especially thankful to Nick Ackerley, Canadian Hazard Information Service, whose constructive comments and thorough checking of the article helped in improving the overall shape of the article.

REFERENCES

Chen, D. Y., N. C. Hsiao, and Y. M. Wu (2015). The Earthworm based earthquake alarm reporting system in Taiwan, *Bull. Seismol. Soc. Am.* **105,** 568–579, doi: 10.1785/0120140147.

Holland, A. (2003). Earthquake data recorded by the MEMS accelerometer: Field testing in Idaho, *Seismol. Res. Lett.* **74,** 20–26, doi: 10.1785/gssrl.74.1.20.

Hsieh, C. Y., W. A. Chao, and Y. M. Wu (2015). An examination of the threshold-based earthquake early warning approach using a low cost seismic network, *Seismol. Res. Lett.* **86,** 1664–1667, doi: 10.1785/0220150073.

Hsieh, C. Y., Y. M. Wu, T. L. Chin, K. H. Kuo, D. Y. Chen, K. S. Wang, Y. T. Chan, W. Y. Chang, W. S. Li, and S. H. Ker (2014). Low cost

seismic network practical applications for producing quick shaking maps in Taiwan, *Terr. Atmos. Ocean. Sci.* **25,** 617–624, doi: 10.3319/TAO.2014.03.27.01(T).
Hsu, T. Y., R. C. Yin, and Y. M. Wu (2018). Evaluating post-earthquake building safety using economical MEMS seismometers, *Sensors* **18,** 1437, doi: 10.3390/s18051437.
Jan, J. C., W. A. Chao, Y. M. Wu, C. C. Chen, and C. H. Lin (2017). How well can we extract the permanent displacement from low-cost MEMS accelerometers?, *Sensors* **17,** 2643, doi: 10.3390/s17112643.
Johnson, C. E., A. Bittenbinder, B. Bogaert, L. Dietz, and W. Kohler (1995). Earthworm: A flexible approach to seismic network processing, *IRIS Newsletter* **14,** 4.
Kalkan, E., and S. K. Kunnath (2006). Effects of fling step and forward directivity on seismic response of buildings, *Earthq. Spectra* **22,** 367–390, doi: 10.1193/1.2192560.
Kumar, A., H. Mittal, B. P. Chamoli, A. Gairola, R. S. Jakka, and A. Srivastava (2014). Earthquake early warning system for northern India, *15th Symposium on Earthquake Engineering*, Indian Institute of Technology, Roorkee, 11–13 December 2014, 231–238.
Lee, S. J., T. C. Lin, T. Y. Liu, and T. P. Wong (2018). Fault-to-fault jumping rupture of the 2018 M_w 6.4 Hualien earthquake in eastern Taiwan, *Seismol. Res. Lett.* (in this issue).
Legendre, C. P., T. L. Tseng, H. Mittal, C. H. Hsu, A. Karakhanyan, and B. S. Huang (2017). Complex wave propagation revealed by peak ground velocity maps in the Caucasus area, *Seismol. Res. Lett.* **88,** 812–821, doi: 10.1785/0220160178.
Mittal, H., A. Kumar, and Kamal(2013). Ground motion estimation in Delhi from postulated regional and local earthquakes, *J. Seismol.* **17,** 593–605, doi: 10.1007/s10950-012-9340-5.
Mittal, H., A. Kumar, Y. M. Wu, Kamal, and A. Kumar (2016). Source study of M_w 5.4 April 4, 2011 India–Nepal border earthquake and scenario events in the Kumaon-Garhwal region, *Arabian J. Geosci.* **9,** 348, doi: 10.1007/s12517-016-2330-0.
Ruiz, S., E. Kausel, J. Campos, G. R. Saragoni, and R. Madariaga (2011). Identification of high frequency pulses from earthquake asperities along Chilean subduction zone using strong motion, *Pure Appl. Geophys.* **168,** 125–139.
Shieh, J. T., Y. M. Wu, and R. M. Allen (2008). A comparison of and for magnitude estimation in earthquake early warning, *Geophys. Res. Lett.* **35,** L20301, doi: 10.1029/2008GL035611.
Shyu, J. B. H., Y. R. Chuang, Y. L. Chen, Y. R. Lee, and C. T. Cheng (2016). A new on-land seismogenic structure source database from the Taiwan earthquake model (TEM) project for seismic hazard analysis of Taiwan, *Terr. Atmos. Ocean. Sci.* **27,** 311–323, doi: 10.3319/TAO.2015.11.27.02(TEM).
Tsai, Y. B., T. L. Teng, J. M. Chiu, and H. L. Liu (1977). Tectonic implications of the seismicity in the Taiwan region, *Mem. Geol. Soc. China* **2,** 13–41.
Wessel, P., and W. H. F. Smith (1998). New, improved version of Generic Mapping Tools released, *Eos Trans. AGU* **79,** 579.
Wikipedia (2018). *2018 Hualien Earthquake*, available at https://en.wikipedia.org/wiki/2018_Hualien_earthquake (last accessed July 2018).
Worden, C. B., E. M. Thompson, J. W. Baker, B. A. Bradley, N. Luco, and D. J. Wald (2018). Spatial and spectral interpolation of ground-motion intensity measure observations, *Bull. Seismol. Soc. Am.* **108,** 866–875.
Worden, C. B., D. J. Wald, T. I. Allen, K. Lin, D. Garcia, and G. Cua (2010). A revised ground-motion and intensity interpolation scheme for ShakeMap, *Bull. Seismol. Soc. Am.* **100,** 3083–3096.
Wu, Y. M. (2015). Progress on development of an earthquake early warning system using low cost sensors, *Pure Appl. Geophys.* **172,** 2343–2351, doi: 10.1007/s00024-014-0933-5.
Wu, Y. M., and H. Kanamori (2005). Rapid assessment of damaging potential of earthquakes in Taiwan from the beginning of P waves, *Bull. Seismol. Soc. Am.* **95,** 1181–1185, doi: 10.1785/0120040193.
Wu, Y. M., and T. L. Lin (2014). A test of earthquake early warning system using low cost accelerometer in Hualien, Taiwan, in *Early Warning for Geological Disasters—Scientific Methods and Current Practice*, F. Wenzel and J. Zschau (Editors), Springer-Berlin-Heidelberg, New York, New York, 253–261, ISBN: 978-3-642-12232-3, doi: 10.1007/978-3-642-12233-0_13.
Wu, Y. M., and C. F. Wu (2007). Approximate recovery of coseismic deformation from Taiwan strong-motion records, *J. Seismol.* **11,** 159–170.
Wu, Y. M., C. H. Chang, L. Zhao, T. L. Teng, and M. Nakamura (2008). A comprehensive relocation of earthquakes in Taiwan from 1991 to 2005, *Bull. Seismol. Soc. Am.* **98,** 1471–1481, doi: 10.1785/0120070166.
Wu, Y. M., C. C. Chen, T. C. Shin, Y. B. Tsai, W. H. K. Lee, and T. L. Teng (1997). Taiwan rapid earthquake information release system, *Seismol. Res. Lett.* **68,** 931–943.
Wu, Y. M., D. Y. Chen, T. L. Lin, C. Y. Hsieh, T. L. Chin, W. Y. Chang, W. S. Li, and S. H. Ker (2013). A high density seismic network for earthquake early warning in Taiwan based on low cost sensors, *Seismol. Res. Lett.* **84,** 1048–1054, doi: 10.1785/0220130085.
Wu, Y. M., J. K. Chung, T. C. Shin, N. C. Hsiao, Y. B. Tsai, W. H. K. Lee, and T. L. Teng (1999). Development of an integrated earthquake early warning system in Taiwan—Case for Hualien earthquakes, *Terr. Atmos. Ocean. Sci.* **10,** 719–736.
Wu, Y. M., N. C. Hsiao, and T. L. Teng (2004). Relationships between strong ground motion peak values and seismic loss during the 1999 Chi-Chi, Taiwan earthquake, *Nat. Hazards* **32,** 357–373.
Wu, Y. M., W. H. K. Lee, C. C. Chen, T. C. Shin, T. L. Teng, and Y. B. Tsai (2000). Performance of the Taiwan rapid earthquake information release system (RTD) during the 1999 Chi-Chi (Taiwan) earthquake, *Seismol. Res. Lett.* **71,** 338–343.
Wu, Y. M., W. T. Liang, H. Mittal, W. A. Chao, C. H. Lin, B. S. Huang, and C. M. Lin (2016). Performance of a low-cost earthquake early warning system (*P*-alert) during the 2016 M_L 6.4 Meinong (Taiwan) earthquake, *Seismol. Res. Lett.* **87,** 1050–1059, doi: 10.1785/0220160058.
Wu, Y. M., T. L. Lin, W. A. Chao, H. H. Huang, N. C. Hsiao, and C. H. Chang (2011). Faster short-distance earthquake early warning using continued monitoring of filtered vertical displacement—A case study for the 2010 Jiasian earthquake, Taiwan, *Bull. Seismol. Soc. Am.* **101,** 701–709, doi: 10.1785/0120100153.
Wu, Y. M., T. L. Teng, T. C. Shin, and N. C. Hsiao (2003). Relationship between peak ground acceleration, peak ground velocity, and intensity in Taiwan, *Seismol. Res. Lett.* **93,** 386–396.
Yang, B. M., T. C. Huang, and Y. M. Wu (2018). ShakingAlarm: A nontraditional regional earthquake early warning system based on time-dependent anisotropic peak ground-motion attenuation relationships, *Bull. Seismol. Soc. Am.* **108,** 1219–1230, doi: 10.1785/0120170105.
Yin, R. C., Y. M. Wu, and T. Y. Hsu (2016). Application of the low-cost MEMS-type seismometer for structural health monitoring: A pre-study, *2016 IEEE International Instrumentation and Measurement Technology Conf. Proceedings (I2MTC)*, 1–5, doi: 10.1109/I2MTC.2016.7520389.
Yu, S. B., H. Y. Chen, and L. C. Kuo (1997). Velocity field of GPS stations in the Taiwan area, *Tectonophysics* **274,** 41–59.

Yih-Min Wu[1]
Himanshu Mittal
Ting-Chung Huang
Benjamin M. Yang
Sean Kuanhsiang Chen
Department of Geosciences
National Taiwan University
Number 1, Section 4, Roosevelt Road

Taipei 10617, Taiwan
drymwu@ntu.edu.tw
himanshumitt10@gmail.com
tingchunghuang@gmail.com
b98204032@gmail.com
sean80254@gmail.com

Jyh-Cherng Jan[2]
Institute of Earth Sciences
Academia Sinica
Number 128, Section 2, Academia Road, Nangang
Taipei 11529, Taiwan
jyhcherngjan@gmail.com

Published Online 5 September 2018

[1] Also at NTU Research Center for Future Earth, National Taiwan University, Taipei 10617, Taiwan; yihmin.wu@gmail.com; and Also at Institute of Earth Sciences, Academia Sinica, Taipei 11529, Taiwan.
[2] Also at Department of Earth Sciences, National Central University, Jhongli 320, Taiwan.